

Synthesis of $\text{Fe}_8\text{V}_{10}\text{W}_{16}\text{O}_{85}$ by a solution method

P. Tabero¹  · A. Frackowiak¹

Received: 15 November 2015 / Accepted: 3 July 2016 / Published online: 25 July 2016
© The Author(s) 2016. This article is published with open access at Springerlink.com

Abstract Phase of block-type structure and formula $\text{Fe}_8\text{V}_{10}\text{W}_{16}\text{O}_{85}$ has been synthesized by a solution method using $\text{Fe}(\text{NO}_3)_3 \cdot 9\text{H}_2\text{O}$, NH_4VO_3 and $(\text{NH}_4)_6\text{W}_{12}\text{O}_{39} \cdot x\text{H}_2\text{O}$ as a metal precursors. Brown solid obtained after evaporation of water at 60 °C has been heated in air at temperatures selected based on results of measurements with the aid of differential thermal analysis and thermogravimetric analysis up to 1000 °C. Products obtained after selected stages of heating have been investigated with the help of X-ray diffraction, infrared spectroscopy and diffusion reflectance spectroscopy in the near-infrared range. Results of investigations have revealed several stages of thermal decomposition of precursor with the FeVO_4 , monoclinic WO_3 and unknown phase as intermediate products. Single-phase sample of $\text{Fe}_8\text{V}_{10}\text{W}_{16}\text{O}_{85}$ has been obtained after heating stage at 800 °C. Tungsten precursor $(\text{NH}_4)_6\text{W}_{12}\text{O}_{39} \cdot x\text{H}_2\text{O}$ has been subjected to thermoanalytical and spectroscopic study as well. Process of thermal decomposition of tungsten precursor runs with formation of hexagonal WO_3 and ammonium bronze $(\text{NH}_4)_{0.33-x}\text{WO}_3$, with monoclinic WO_3 as a final product of decomposition.

Keywords $\text{Fe}_8\text{V}_{10}\text{W}_{16}\text{O}_{85}$ · Solution method · DTA–TG · XRD · IR · NIR/DRS

Introduction

Selective catalytic oxidation (SCO) of ammonia and oxidative dehydrogenation (ODH) of light hydrocarbons have been extensively studied over alumina- or titania-supported vanadium or iron oxide catalysts [1–4]. A major challenge in this field is improvement of selectivity and reduction of temperature of catalytic process. One method to overcome these problems is to use metal oxide additives. The vanadium-containing catalysts can be tuned with second or third component like W, Mo, Fe, Ni and Co [1–4]. Another interesting problem to solve is to search for new and effective materials for manufacturing of electrodes in secondary lithium batteries. Such materials should have in their structure tunnels, which can serve as the paths of easy diffusion of lithium during charging and discharging of batteries. Potential candidate for manufacturing of both catalysts and electrodes is phase $\text{Fe}_8\text{V}_{10}\text{W}_{16}\text{O}_{85}$ forming in the system Fe_2O_3 – V_2O_5 – WO_3 [5–9]. $\text{Fe}_8\text{V}_{10}\text{W}_{16}\text{O}_{85}$ crystallizes in a tetragonal system and adopts $\text{M-Nb}_2\text{O}_5$ tunnel structure [5, 6]. Its unit cell parameters are following: $a = b = 1.9753$ nm, $c = 0.3717$ nm [5, 6]. This compound melts at 840 °C with depositing two solid products, i.e., WO_3 and Fe_2WO_6 [8]. It is also known that in the system Fe_2O_3 – V_2O_5 – WO_3 – MoO_3 solid solution of type $\text{Fe}_8\text{V}_{10}\text{W}_{16-x}\text{Mo}_x\text{O}_{85}$ is formed (for $x \leq 4$), which is isostructural with $\text{Fe}_8\text{V}_{10}\text{W}_{16}\text{O}_{85}$ [7]. The literature scan has shown that $\text{Fe}_8\text{V}_{10}\text{W}_{16}\text{O}_{85}$ can be obtained in the solid state, but at temperatures higher than 700 °C [9]. The aim of this work was searching for alternative synthesis methods for $\text{Fe}_8\text{V}_{10}\text{W}_{16}\text{O}_{85}$ that would allow its preparation at significantly lower temperatures. This paper presents results of investigations concerning synthesis of $\text{Fe}_8\text{V}_{10}\text{W}_{16}\text{O}_{85}$ by the solution method. The properties of tungsten

✉ P. Tabero
ptab@zut.edu.pl

¹ Department of Inorganic and Analytical Chemistry, Faculty of Chemical Engineering, West Pomeranian University of Technology, Szczecin, Al. Piastow 42, 71-065 Szczecin, Poland

precursor $(\text{NH}_4)_6\text{W}_{12}\text{O}_{39}\cdot x\text{H}_2\text{O}$ used for preparation of $\text{Fe}_8\text{V}_{10}\text{W}_{16}\text{O}_{85}$ have been subjected to study as well.

Experimental

For the synthesis of $\text{Fe}_8\text{V}_{10}\text{W}_{16}\text{O}_{85}$ by the solution method, the following metal precursors were used: $\text{Fe}(\text{NO}_3)_3\cdot 9\text{H}_2\text{O}$ a.p. (Chempur, Poland), NH_4VO_3 a.p. (POCH Gliwice, Poland) and $(\text{NH}_4)_6\text{W}_{12}\text{O}_{39}\cdot x\text{H}_2\text{O}$ (Aldrich, Germany). In the text of this paper, tungsten precursor $(\text{NH}_4)_6\text{W}_{12}\text{O}_{39}\cdot x\text{H}_2\text{O}$ will be denoted as WP. As the water content in $(\text{NH}_4)_6\text{W}_{12}\text{O}_{39}\cdot x\text{H}_2\text{O}$ was unknown, the WO_3 content in tungsten precursor was established based on the results of DTA–TG investigations. For the synthesis of $\text{Fe}_8\text{V}_{10}\text{W}_{16}\text{O}_{85}$ by the solution method, three solutions in distilled water were prepared: 5.7406 g of $\text{Fe}(\text{NO}_3)_3$ in 60 cm³ of water, 6.5474 g of WP in 60 cm³ of water and 1.8911 g of NH_4VO_3 in 400 cm³ of water. Received solutions were mixed together with energetic stirring. Obtained in this way light orange solution was evaporated to dryness at 60 °C yielding brown solid. In the text of this paper such obtained solid product will be denoted as FeVW. To know the mechanism of decomposition of FeVW, 2 g samples of FeVW was calcined in independent experiments at 190, 300, 600, 750 and 800 °C in 1-h stages and at 800 °C for 24 h. In the parallel studies, tungsten precursor WP was calcined in independent experiments at 190, 375 and 600 °C in 1-h stages. The temperatures of calcinations of samples were selected based on the results of DTA–TG investigations of WP and FeVW. The phase composition and properties of substrates and products obtained after each heating stage were established using XRD, IR and NIR/DRS instrumental techniques.

X-ray phase analysis (XRD) of the samples was performed using an Empyrean II diffractometer (PANalytical, The Netherlands) applying copper tube equipped with a graphite monochromator. The identification of the individual phases was performed by using HighScore software (PANalytical, The Netherlands) and ICDD PDF4+ 2014 database.

The IR spectra were recorded by Specord M80 spectrometer (Carl Zeiss, Jena, Germany) using pellets in KBr at a mass ratio 1:300.

The NIR/DRS measurements were made using a Jasco V670 spectrometer matched with integrating sphere PIN 757 (Jasco, Japan) using Spectralon as a reference material.

The DTA–TG examinations were performed using an apparatus SDT 2960 (TA Instruments, USA). Samples of 25 mg were investigated up to 1000 °C in static air in quartz crucibles and at the heating rate of 10 °C min⁻¹.

Results and discussion

Hunyadi and coworkers [10] investigated lately commercial samples of $(\text{NH}_4)_6\text{W}_{12}\text{O}_{39}\cdot x\text{H}_2\text{O}$ (AMT1) and $(\text{NH}_4)_6[\text{H}_2\text{W}_{12}\text{O}_{40}]\cdot x\text{H}_2\text{O}$ (AMT2) and shown that both products have identical powder diffraction patterns and crystallize in an orthorhombic system. On the other hand, based on results of DTA–TG investigations, authors attributed $(\text{NH}_4)_6[\text{H}_2\text{W}_{12}\text{O}_{40}]\cdot 4\text{H}_2\text{O}$ formula for both samples and concluded that real chemical formulas and compositions of commercial reactants from metatungstate group can differ from formulas provided by their manufacturer [10]. To check these facts in the first stage of investigation used by them, tungsten precursor $(\text{NH}_4)_6\text{W}_{12}\text{O}_{39}\cdot x\text{H}_2\text{O}$ (WP) and products of its decomposition at selected temperatures were subjected to XRD, DTA–TG, IR and NIR/DRS investigations.

Results of our XRD investigations have revealed that powder diffraction pattern of tungsten precursor WP, $(\text{NH}_4)_6\text{W}_{12}\text{O}_{39}\cdot x\text{H}_2\text{O}$ (Fig. 1, curve a), used by them differs considerably in respect of number of reflections, their angular positions and intensities from these ones characteristic for AMT1 and AMT2 samples for which Hunyadi and coworkers attributed formula $(\text{NH}_4)_6[\text{H}_2\text{W}_{12}\text{O}_{40}]\cdot 4\text{H}_2\text{O}$. Additionally, diffraction pattern of WP was not consistent with any single diffraction pattern of ammonium tungstate(VI) included in PDF-4 2014 database.

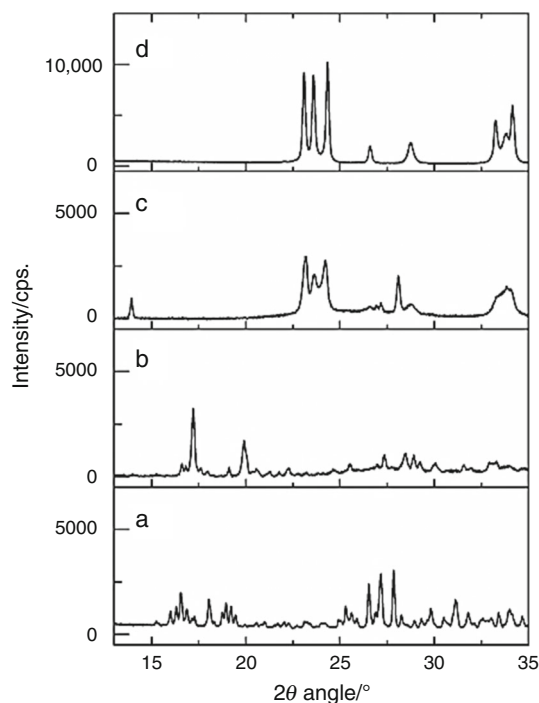


Fig. 1 Fragments of powder diffraction patterns of WP (a) and products obtained after its heating at 190 °C (b), 375 °C (c) and 600 °C (d)

In order to know WO_3 content in WP, sample of tungsten precursor was subjected to DTA–TG investigations. Figure 2 shows DTA and TG curves of WP. The DTA–TG curves have complex shape comprising a series of processes quickly following one another. One can distinguish five mass loss stages on the TG curve. On the DTA curve were recorded three endothermic and two exothermic effects. The first and second mass loss processes start at 40 and at 60 °C, respectively, and run with mass loss of 3.0 and 2.0 %, respectively. Both processes are accompanied by endothermic effects. Mass loss recorded in this stage of decomposition of WP (5.0 mass %) is considerably greater than the mass loss (2.4 mass %) recorded in analogous stage of decomposition by Hunyadi et al. [10]. The third stage of investigated process commences at 220 °C, runs with 4.5 % mass loss and is also accompanied by endothermic effect. The fourth and fifth mass loss processes start at 350 and 450 °C, respectively, and are accompanied by exothermic effects. The overall mass loss for both processes equals to 0.8 %. These mass loss effects are comparable with analogous effects recorded by Hunyadi et al. [10] and equal to 4.2 and 0.9 mass%. Thus, results of TG investigations have revealed that decomposition of WP runs with overall mass loss of 10.3 % which indicates that it contains 89.7 % WO_3 . This overall mass loss is greater than the mass loss recorded for $(\text{NH}_4)_6[\text{H}_2\text{W}_{12}\text{O}_{40}]\cdot 4\text{H}_2\text{O}$ (8.1 %) [10] which proves that WP has different empirical formula.

In order to get insight into decomposition process of WP, samples of tungsten precursor were heated at 190, 375 and 600 °C in 1-h stages. Fragments of powder diffraction

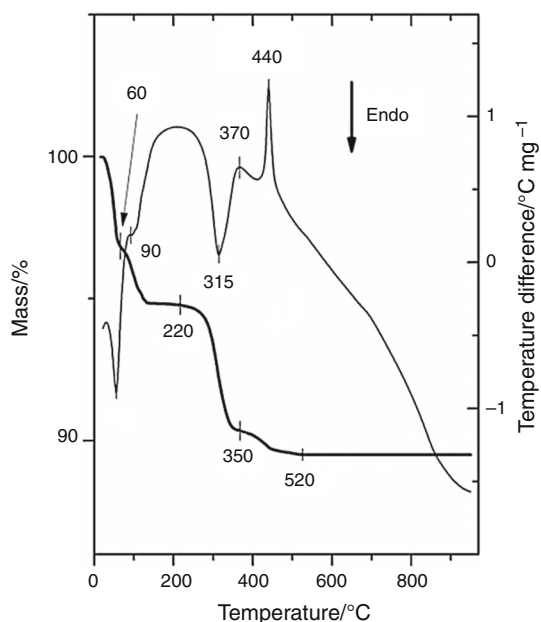


Fig. 2 DTA (–) and TG (—) curves of WP

patterns recorded after each stage of heating are shown in Fig. 1. Diffraction pattern recorded after heating at 190 °C (curve b) differs considerably from this one of WP (curve a) and any single diffraction pattern of ammonium tungstate(VI) included in PDF-4 2014 database. On the other hand, X-ray phase analysis has revealed that diffraction pattern of WP sample after heating at 375 °C comprises a set of diffraction reflections which can be attributed to hexagonal WO_3 (h- WO_3 , PDF 04-007-2322) and monoclinic WO_3 (m- WO_3 , PDF 00-043-1035) [10–12]. We can't exclude, however, content of hexagonal ammonium tungsten bronze $(\text{NH}_4)_{0.33-x}\text{WO}_{3-y}$ (HATB, PDF 00-058-0151) in this sample because there is no sharp division of diffraction reflections between h- WO_3 and HATB [10, 13, 14]. Powder diffraction pattern of WP sample heated at 600 °C comprised only diffraction reflections characteristic for monoclinic WO_3 [10–12, 14]. Formation of m- WO_3 as an end product of decomposition of WP corroborates our earlier statement that WP contains 89.7 mass% of WO_3 .

Next, samples of pure WP and WP heated at 190, 375 and 600 °C in 1-h stages were subjected to investigations with the help of IR and NIR/DRS spectroscopic methods. Figure 3 shows IR spectra and Fig. 4 NIR/DRS spectra of investigated samples matched with spectrum of starting WP. IR and NIR spectroscopic techniques are closely

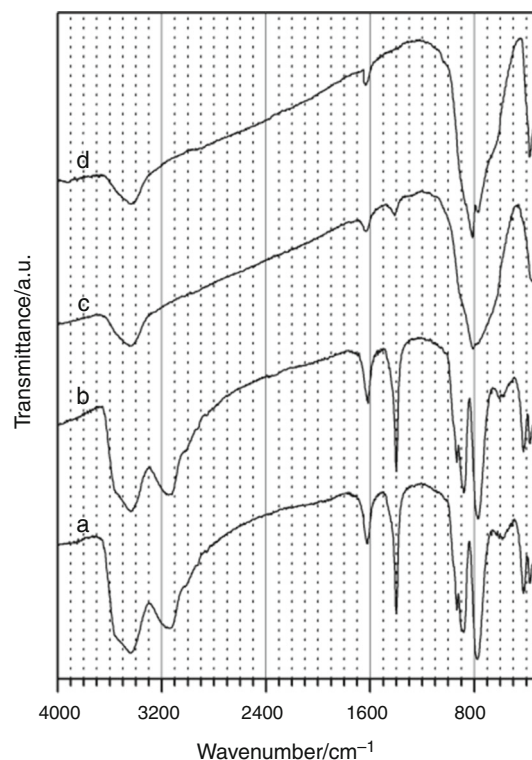


Fig. 3 IR spectra of WP (a) and products obtained after its heating at 190 °C (b), 375 °C (c) and 600 °C (d)

related. Molecular functional groups like O–H or N–H absorb radiation in the mid-IR with considerably weaker overtones, and combination vibrations detected in both the mid-IR and NIR regions [10, 14–23]. IR absorption spectra are, however, frequently obscured by vibrations produced by water adsorbed during preparation of KBr pellets. Manner of preparation of samples for measurements using diffusion reflectance method (NIR/DRS), when the just obtained samples can be investigated without any preliminary processing led one to avoid this problem. Thus, results of NIR/DRS measurements can help to interpret IR spectra of samples containing water or OH groups. Water has strong characteristic absorptions near 1400 and 1900 nm, which are accompanied by weaker bands near 760, 970 and 1200 nm [15–19]. Moreover, combination vibrations involving a O–H stretch and metal–OH bend can occur in the 2200- to 2500-nm region, with bands at 2200 and 2300 nm characteristic for Al–OH and Fe–OH groups, respectively [17–19]. On the other hand, three main bands of ammonia occur at 1.5, 2.0 and 2.3 μm [18–23]. Thus, absorption bands characteristic for N–H and O–H groups are shifted mutually enabling identification and distinction of both groups in IR and NIR/DRS spectra.

IR spectra of starting WP and sample obtained after heating WP at 190 °C are very similar in respect of number of bands and their intensities and comprise bands characteristic for water (maxima at 1630 and 3440 cm^{-1}) and ammonia (1400 and 3130 cm^{-1}). Despite the fact that NIR/DRS spectra of WP and WP calcined at 190 °C contain absorptions characteristic for H₂O (970, 1175, 1430 and

1930 nm) and ammonia (1575, 2040 and 2150 nm), intensity of bands is lower in the case of sample of WP heated at 190 °C. It indicates that the first and second mass loss processes (onsets at 40 and 60 °C) are connected mainly with elimination of water. IR spectrum of WP heated at 375 differs considerably from spectra of WP and WP heated at 190 °C. This spectrum does not comprise strong band at 3130 cm^{-1} characteristic for ammonia. However, weak absorption band at 1400 cm^{-1} indicates the presence of small amounts of ammonia (NH₄ groups) in this sample. Absorption bands at 1630 and 3440 cm^{-1} are much weaker than in the case of spectra of pure WP and WP heated at 190 °C. Such bands are most probably produced by water molecules adsorbed by KBr in the course of preparation of KBr pellets or small amounts of water adsorbed on the surface layer of obtained product. This suggestion is supported by the results of NIR/DRS investigations. NIR/DRS spectrum of WP sample heated at 375 °C comprises only absorption bands characteristic for ammonia (1575, 2040 and 2150 nm). Intensity of absorption bands characteristic for ammonia (NH₄ groups) is weak, indicating low ammonia content in the sample. Low content of ammonia in this sample is in accord with low mass loss (0.8 %) recorded on TG curve in the temperature range of 350–520 °C. An exothermic effect recorded on DTA curve with maximum at 370 °C is most probably related to transformation of amorphous phase to h-WO₃ or HATB, whereas this at 440 °C can be connected with combustion of ammonia [10, 14]. IR and NIR/DRS spectra of WP sample heated at 600 °C do not include absorption bands characteristic for ammonia and water (IR bands at 3440 and 1630 cm^{-1} are produced by water adsorbed by KBr), supporting results of XRD investigations, indicating that this sample contains pure m-WO₃. IR bands recorded in the range of 1000–300 cm^{-1} on all spectra in Fig. 3 can be ascribed to stretching vibrations of W–O bonds in distorted WO_x polyhedra present in obtained phases [5, 6, 10, 14].

In the second stage of research, brown solid obtained after evaporation of water at 60 °C from solution containing metal precursors of iron, vanadium and tungsten (FeVW) and products obtained after its heating at 190, 300, 600, 750 and 800 °C were subjected to XRD, DTA–TG, IR and NIR/DRS investigations. Figure 5 shows DTA and TG curves of FeVW. Mass loss process (TG curve, Fig. 5) can be divided into three stages. On the other hand, on DTA curve were recorded three endothermic effects and one exothermic. The first mass loss process starts at 60 °C and ends at 200 °C, runs with mass loss of 11.1 % and is accompanied by endothermic effect. The second stage commences at 200 °C and ends at 300 °C, runs with 20.3 % mass loss but is accompanied by exothermic effect. The third mass loss process connected with mass loss of

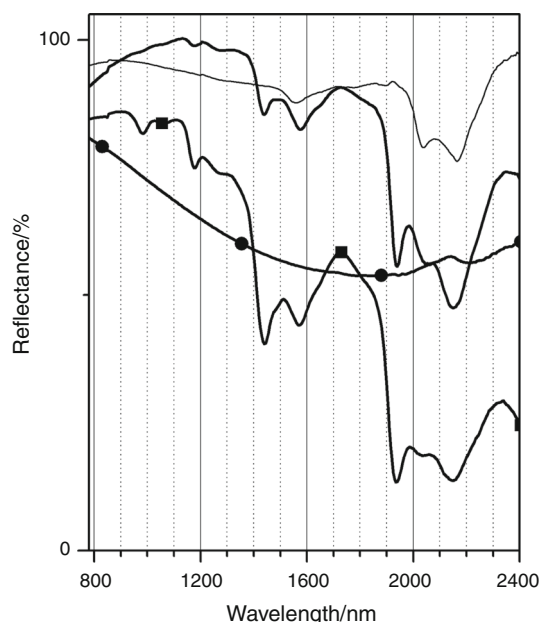


Fig. 4 NIR/DRS spectra of WP (square) and products obtained after its heating at 190 °C (– · –), 375 °C (– –) and 600 °C (circle)

0.6 % starts at 530 °C and ends at 580 °C and is not accompanied by any well-defined thermal effects. Thus, decomposition of FeVW runs with overall mass loss of 32.0 %. Moreover, on the DTA curve were recorded also two weak endothermic effects with maxima at 820 and 840 °C. The first effect can be attributed to melting of $\text{Fe}_8\text{V}_{10}\text{W}_{16}\text{O}_{85}$ [8] and the second one to melting of FeVO_4 [24] which were formed in small amounts in the course of heating the sample. In order to get insight into decomposition process of FeVW, samples of FeVW were heated at 190, 300, 600, 750 and 800 °C in 1-h stages and at 800 °C for 24 h.

Powder diffraction patterns of FeVW recorded after each stage of heating are shown in Fig. 6. Results of XRD investigations revealed that FeVW sample besides amorphous component contains also small amount of crystalline NH_4NO_3 , the by-product of the synthesis. Figure 6 (curve a) shows fragment of this powder diffraction pattern. Analysis of recorded powder diffraction patterns points out that decomposition process of FeVW runs through the stage with formation of amorphous product (Fig. 6, curve b, heating at 190 °C), formation of mixture of unknown phase and FeVO_4 (PDF 04-008-387) (Fig. 6, curve c, heating at 300 °C, and curve d, heating at 600 °C) and formation of mixture of m-WO_3 and FeVO_4 (Fig. 6, curve e, heating at 750 °C and stage after heating at 800 °C for 1 h, pattern not shown in Fig. 6). The results of XRD investigations have revealed that only heating at 800 °C for 24 h (Fig. 6, curve f) was effective and gave a pure sample of crystalline $\text{Fe}_8\text{V}_{10}\text{W}_{16}\text{O}_{85}$. This fact is in accord with data presented in work [9] that $\text{Fe}_8\text{V}_{10}\text{W}_{16}\text{O}_{85}$ can be obtained in the solid

state at temperatures higher than 700 °C. Results of XRD investigations show, however, that short-time heating at 750 and at 800 °C is not effective for synthesis of detectable by XRD amounts of crystalline $\text{Fe}_8\text{V}_{10}\text{W}_{16}\text{O}_{85}$ (Fig. 6).

Samples of FeVW and FeVW heated at 190, 300, 600, 750 and 800 °C were subjected to investigations using IR and NIR/DRS spectroscopy. Recorded spectra are shown in Fig. 7 (IR spectra) and in Fig. 8 (NIR/DRS spectra).

Similarly like in the case of WP, IR spectra of FeVW (Fig. 7, curve a) and FeVW after heating at 190 °C (Fig. 7, curve b) are very similar and include absorption bands characteristic for ammonia (maxima at 1400 and 3130 cm^{-1}) and water (maxima at 1630 and 3440 cm^{-1}). On the other hand, analysis of NIR/DRS spectra of these samples (Fig. 8, curves a, b) shows that after calcinations at 190 °C intensity of bands characteristic for water (1430 and 1930 nm) decreased considerably, whereas these ones characteristic for ammonia (1575, 2040 and 2150 nm) did not changed their intensities. It indicates that the first mass loss process (onset at 60 °C) is mainly connected with elimination of water from FeVW. NIR/DRS spectrum of FeVW sample heated at 300 °C (Fig. 8, curve denoted as triangle) does not contain bands characteristic for water and ammonia, whereas IR spectrum comprises only a very weak band characteristic for ammonia (1400 cm^{-1}). It points out that at second stage of decomposition (onset at 200 °C) ammonia is evolved. Further heating of samples at

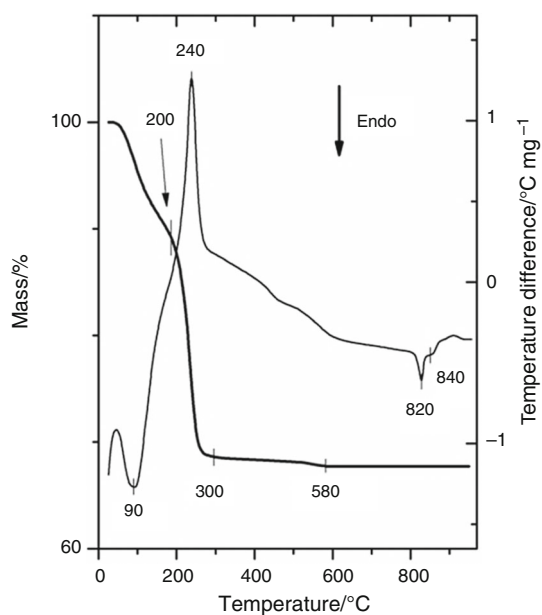


Fig. 5 DTA (—) and TG (---) curves of FeVW

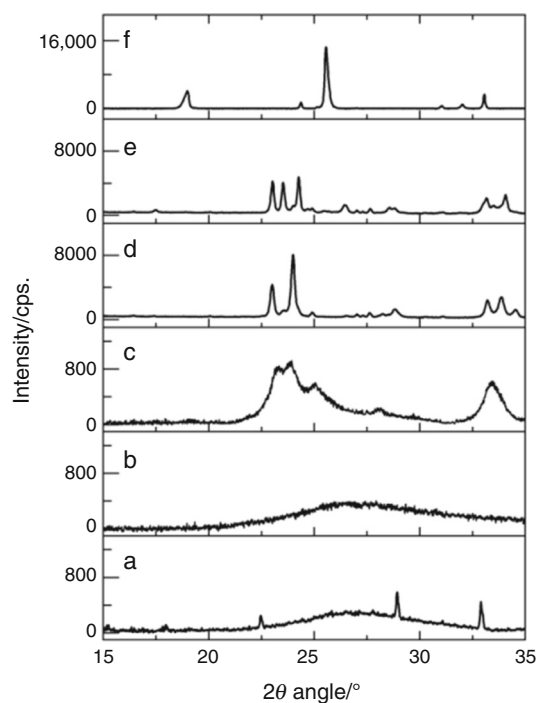


Fig. 6 Fragments of powder diffraction patterns of FeVW (a) and products obtained after its heating at 190 °C (b), 300 °C (c), 600 °C (d), 750 °C (e) and 800 °C for 24 h (f)

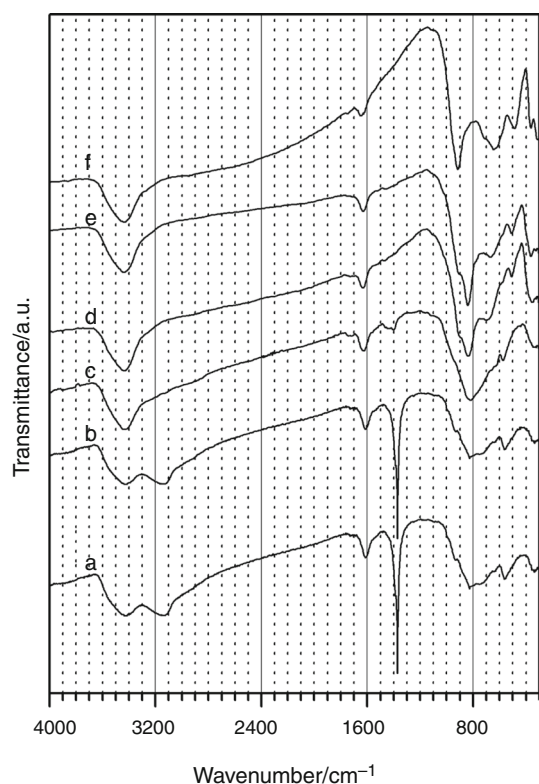


Fig. 7 IR spectra of FeVW (a) and products obtained after its heating at 190 °C (b), 300 °C (c), 600 °C (d), 750 °C (e) and 800 °C for 24 h (f)

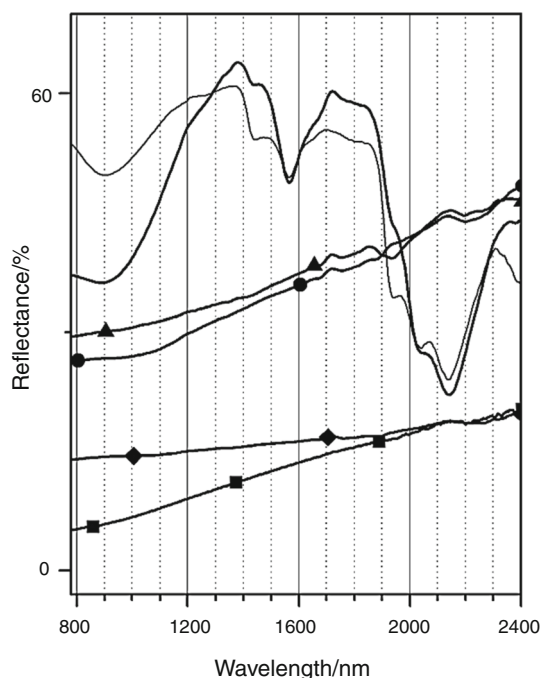


Fig. 8 NIR/DRS spectra of FeVW (—) and products obtained after its heating at 190 °C (---), 300 °C (triangle), 600 °C (circle), 750 °C (diamond) and 800 °C for 24 h (square)

higher temperatures changes mainly the envelope of IR spectra in the 1000–300 cm^{-1} range, characteristic for absorption of radiation by WO_x polyhedra [5, 6, 10, 14], and shifts NIR/DRS curves toward lower values of reflectance. This last phenomenon can be connected with gradual change in color of samples from brown to almost black, characteristic for samples after heating at 800 °C.

Analysis of results obtained during investigation of tungsten precursor WP and brown solid FeVW indicates that exothermic effects recorded on DTA curves of WP and FeVW can be attributed to oxidation of ammonia [10, 14, 25–27]. It is worth to say that strong exothermic effect recorded on DTA curve of WP with maximum at 440 °C is shifted in the case of FeVW toward lower temperatures with maximum at 240 °C. According to literature data, NH_4NO_3 , which was detected in FeVW sample, melts at 169.6 °C and then starts to dissociate into NH_3 and HNO_3 [25–27]. Next, NH_3 is oxidized by decomposition products of HNO_3 . In the temperature range of 200–230 °C exothermic decomposition occurs. Thus, exothermic effect recorded on DTA curve of FeVW with maximum at 240 °C can be attributed to oxidation of ammonia, product of decomposition of NH_4NO_3 . It seems that admixtures of vanadium or vanadium, iron and tungsten can play the role of catalysts in oxidation of ammonia and are responsible for lowering the temperature of ammonia oxidation.

Conclusions

1. $\text{Fe}_8\text{V}_{10}\text{W}_{16}\text{O}_{85}$ has been synthesized by a solution method using $\text{Fe}(\text{NO}_3)_3 \cdot 9\text{H}_2\text{O}$, NH_4VO_3 and $(\text{NH}_4)_6\text{W}_{12}\text{O}_{39} \cdot x\text{H}_2\text{O}$ as a metal precursors.
2. Process of decomposition of metal precursors is complex and runs through the formation of FeVO_4 , monoclinic WO_3 and unknown phase as intermediate products.
3. Single-phase sample of $\text{Fe}_8\text{V}_{10}\text{W}_{16}\text{O}_{85}$ has been obtained after heating stage at 800 °C.
4. Process of decomposition of tungsten precursor $(\text{NH}_4)_6\text{W}_{12}\text{O}_{39} \cdot x\text{H}_2\text{O}$ is also complex and yields at 600 °C monoclinic WO_3 with formation of hexagonal modification of WO_3 and ammonium bronze $(\text{NH}_4)_{0.33-x}\text{WO}_{3-y}$ as intermediate products.

Open Access This article is distributed under the terms of the Creative Commons Attribution 4.0 International License (<http://creativecommons.org/licenses/by/4.0/>), which permits unrestricted use, distribution, and reproduction in any medium, provided you give appropriate credit to the original author(s) and the source, provide a link to the Creative Commons license, and indicate if changes were made.

References

1. Zhang L, He H. Mechanism of selective catalytic oxidation of ammonia to nitrogen over $\text{Ag}/\text{Al}_2\text{O}_3$. *J Catal.* 2009;268:18–25.
2. Jablonska M, Chmielarz L, Wegrzyn A. Selective catalytic oxidation (SCO) of ammonia into nitrogen and water vapour over hydroxalite originated mixed metal oxides, a short review. *Chemik.* 2013;67:701–10.
3. Guerrero-Perez MO, Herrera MC, Malpartida I, Larrubia MA, Alemany LJ. Characterization and FT-IR study of nanostructured alumina-supported V-Mo-W-O catalysts. *Catal Today.* 2006;118:360–5.
4. Mitra B, Wachs IE, Deo G. Promotion of the propane ODH reaction over supported $\text{V}_2\text{O}_5/\text{Al}_2\text{O}_3$ catalyst with secondary surface metal oxide additives. *J Catal.* 2006;240:151–9.
5. Tabero P. Formation and properties of the new $\text{Al}_8\text{V}_{10}\text{W}_{16}\text{O}_{85}$ and $\text{Fe}_{8-x}\text{Al}_x\text{V}_{10}\text{W}_{16}\text{O}_{85}$ phases with M-Nb 2O_5 structure. *J Therm Anal Calorim.* 2010;101:561–6.
6. Rychłowska-Himmel I, Tabero P. Phase equilibria in the system $\text{V}_2\text{O}_5\text{--Fe}_8\text{V}_{10}\text{W}_{16}\text{O}_{85}$ and some properties of the $\text{Fe}_8\text{V}_{10}\text{W}_{16}\text{O}_{85}$ phase. *J Therm Anal Calorim.* 2001;65:537–43.
7. Tabero P. Formation and properties of the $\text{Fe}_8\text{V}_{10}\text{W}_{16-x}\text{Mo}_x\text{O}_{85}$ type solid solution. *J Therm Anal Calorim.* 2007;88:37–41.
8. Rychłowska-Himmel I. Phase equilibria in the system $\text{Fe}_2\text{O}_3\text{--V}_2\text{O}_5\text{--WO}_3$ in the solid state. *J Therm Anal Calorim.* 2000;60:173–85.
9. Walczak J, Rychłowska-Himmel I, Tabero P. Reaction mechanism of $\text{Fe}_8\text{V}_{10}\text{W}_{16}\text{O}_{85}$ synthesis. *J Therm Anal Calorim.* 1999;56(1):419–22.
10. Hunyadi D, Sajo I, Szilágyi IM. Structure and thermal decomposition of ammonium metatungstate. *J Therm Anal Calorim.* 2014;116(1):329–37.
11. Nagy D, Nagy D, Szilágyi IM, Fan X. Effect of the morphology and phases of WO_3 nanocrystals on their photocatalytic efficiency. *RSC Adv.* 2016;6:33743–54.
12. Chacon C, Rodriguez-Perez M, Oskam G, Rodriguez-Gattorno G. Synthesis and characterization of WO_3 polymorphs: monoclinic, orthorhombic and hexagonal structures. *J Mater Sci Mater Electron.* 2015;26:5526–31.
13. Szilágyi IM, Hange F, Madarasz J, Pokol G. In situ HT-XRD study of hexagonal ammonium tungsten bronze by partial reduction of ammonium paratungstate tetrahydrate. *Eur J Inorg Chem.* 2006;17:3413–18.
14. Madarasz J, Szilágyi IM, Hange F, Pokol G. Comparative evolved gas analyses (TG-FTIR, TG/DTA-MS) and solid state (FTIR, XRD) studies on thermal decomposition of ammonium paratungstate tetrahydrate (ATP) in air. *J Therm Anal Calorim.* 2004;72:197–201.
15. Liu WD, Baret F, Gu XF, Tong QX, Zheng LF, Zhang B. Relating soil surface moisture to reflectance. *Remote Sens Environ.* 2002;81:238–46.
16. Zhang Q, Li Q, Zhang G. Rapid determination of leaf water content using VIS/NIR spectroscopy analysis with wavelength selection. *J Spectrosc.* 2012;27:93–105.
17. Rossel RAV, Behrens T. Using data mining to model and interpret soil diffuse reflectance spectra. *Geoderma.* 2010;158:46–54.
18. Buzatu A, Dill HG, Buzgar A, Apopei AI. Efflorescent sulfates from Baia Sprie mining area (Romania)—acid mine drainage and climatological approach. *Sci Total Environ.* 2016;542:629–41.
19. Aenugu HPR, Kumar DS, Srisudharson NP, Ghosh SS, D D. Near infra red spectroscopy—an overview. *Int J ChemTech Res.* 2011;3:825–36.
20. ViscarraRossel RA, McGlynn RN, McBratney AB. Determining the composition of mineral-organic mixes using UV–vis–NIR diffuse reflectance spectroscopy. *Geoderma.* 2006;137:70–82.
21. Takeuchi M, Tsukamoto T, Kondo A, Matsuoka M. Investigation of NH_3 and NH_4^+ adsorbed on ZSM-5 zeolites by near and middle infrared spectroscopy. *Catal Sci Technol.* 2015;5:4587–93.
22. Raju CS, Løkke MM, Sutaryo S, Ward AJ, Møller HB. NIR monitoring of ammonia in anaerobic digesters using a diffuse reflectance probe. *Sensors.* 2012;12:2340–50.
23. Webber ME, Baer DS, Hanson RK. Ammonia monitoring near $1.5\ \mu\text{m}$ with diode-laser absorption sensors. *Appl Opt.* 2001;40:2031–42.
24. Tabero P. Synthesis and properties of $\text{Fe}_{0.83}\text{V}_{1.17}\text{O}_4$. *J Therm Anal Calorim.* 2013;113:247–52.
25. Chaturvedi S, Dave PN. Review on thermal decomposition of ammonium nitrate. *J Energ Mater.* 2013;31(1):1–26.
26. Koga N, Tanaka H. Effect of sample mass on the kinetic of thermal decomposition of a solid. Part 1. Isothermal mass-loss process of molten NH_4NO_3 . *Thermochim Acta.* 1992;209:127–34.
27. Koga N, Tanaka H. Effect of sample mass on the kinetic of thermal decomposition of a solid. Part 3. Non-isothermal mass-loss process of molten NH_4NO_3 . *Thermochim Acta.* 1994;240:141–51.